JOURNAL OF GUIDANCE, CONTROL, AND DYNAMICS
Vol. 28, No. 3, May–June 2005

Attitude Control System of the Wilkinson Microwave Anisotropy Probe

F. Landis Markley,* Stephen F. Andrews,† James R. O'Donnell Jr.,‡ and David K. Ward§
NASA Goddard Space Flight Center, Greenbelt, Maryland 20771

The Wilkinson Microwave Anisotropy Probe mission produces a map of the cosmic microwave background radiation over the entire celestial sphere by executing a fast spin and a slow precession of its spin axis about the sun line to obtain a highly interconnected set of measurements. The attitude control system implements this spin–scan observing strategy while minimizing thermal and magnetic fluctuations, especially those synchronous with the spin period. The spacecraft attitude is sensed and controlled using an inertial reference unit, 2 star trackers, a dual-head digital sun sensor, 12 coarse sun sensors, 3 reaction wheel assemblies, and a propulsion system. Sufficient attitude knowledge is provided to yield instrument pointing to a standard deviation (1σ) of 1.3 arc-min per axis. The attitude control system also maintains the spacecraft attitude during orbit maneuvers, controls the spacecraft angular momentum, and provides for safety in the event of an anomaly. An overview of the design of the attitude control system to carry out this mission is presented, as well as some early flight experience.

Introduction

THE Wilkinson Microwave Anisotropy Probe (WMAP), the second Medium-Class Explorer (MIDEX) mission, was launched on 30 June 2001 as a follow-on to the Cosmic Background Explorer (COBE), which made precise measurements of the cosmic microwave background (CMB) that is believed to be a remnant of the big bang marking the birth of the universe.[1–4] WMAP has measured the CMB anisotropy with sensitivity 50 times that of the differential microwave radiometer (DMR) instrument on COBE and angular resolution 30 times finer, specifically 20 μK and 14 arc-min, respectively, enabling scientists to determine the values of key cosmological parameters and to answer questions about the origin of structure in the early universe and the fate of the universe.[5,6]

Because the major error sources in the DMR data arose from COBE's low Earth orbit, WMAP was placed in a Lissajous orbit around the sun–earth L_2 Lagrange point to minimize magnetic, thermal, and radiation disturbances from the Earth and sun. WMAP attained its Lissajous orbit around L_2 in early October 2001, about 100 days after launch by a Delta II launch vehicle, using a lunar gravity assist following three phasing loops, as shown in Fig. 1. The L_2 Lagrange point is an unstable equilibrium point, and so propulsive maneuvers are required to keep WMAP on station. These are performed no more than twice per orbit (once every three months) to minimize interruptions of science observations. The trajectory design and operations are discussed in detail in Refs. 7–12.

The WMAP instrument includes radiometers at five frequencies, passively cooled to about 90 K, covering two fields of view (FOV) with centers 141 deg apart on the celestial sphere. The WMAP observatory executes a fast spin coupled with a slower precession of its spin axis at a constant angle of 22.5 deg from the sun line to obtain a highly interconnected set of measurements over an annulus between 87 and 132 deg from the sun. The desired degree of interconnection required the rotation about the spin axis to be at least an order of magnitude faster than the rate of precession of the spin axis; the rates chosen were 2.784 deg/s (0.464 rpm) for the spin rate and -0.1 deg/s (1 revolution per hour) for the precession rate. Figure 2 shows the scan pattern covered by one of the two FOV in one complete spacecraft precession (1 h), displayed in ecliptic coordinates in which the ecliptic equator runs horizontally across the map. As the Earth revolves around the sun, this annulus of coverage revolves about the ecliptic pole as shown in Fig. 3. Thus a complete observation of the entire celestial sphere requires slightly less than six months, yielding eight complete observations in the planned mission life of four years.

The spin–scan observing motion is obtained by moving the entire spacecraft rather than by articulating the instrument or antennas, following the example of COBE. This results in much less complex mechanical and thermal designs, avoiding both potential single-point failures and additional heat loads to the cold instrument that would be introduced by moving mechanisms. Other than a one-time-only deployment of the solar arrays, the only moving parts on WMAP are reaction wheels that serve the dual function of counterbalancing the body's spin angular momentum to maintain near-zero total system angular momentum, that is, body plus wheels, while simultaneously applying control torques to provide the desired spin–scan motion.

This paper describes the attitude control system (ACS) that acquires and maintains the spacecraft orbit, controls the spacecraft angular momentum, provides for safety in the event of an anomaly, and implements the spin–scan observing strategy while minimizing thermal and magnetic fluctuations, especially those synchronous with the spin period. It begins with a general overview of the spacecraft layout, ACS architecture, ACS hardware, and momentum management strategy. This is followed by a description of the six ACS control modes, with emphasis on the mode used to perform science observations, using actual flight data to illustrate system performance. Conclusions are drawn in the final section. More detail may be found in Refs. 13–19.

ACS Overview

WMAP uses three reference frames. The Earth-centered inertial frame (ECI) has its $\boldsymbol{x}_I$ axis pointing to the vernal equinox, its $\boldsymbol{z}_I$ axis pointing to the north celestial pole (parallel to the Earth's spin axis), and $\boldsymbol{y}_I = \boldsymbol{z}_I \times \boldsymbol{x}_I$. The rotating sun referenced frame (RSR) is a spacecraft-centered frame in which the $\boldsymbol{z}_R$ axis points from the WMAP spacecraft to the Sun, $\boldsymbol{x}_R$ is a unit vector in the direction of $\boldsymbol{z}_R \times \boldsymbol{z}_I$, and $\boldsymbol{y}_R = \boldsymbol{z}_R \times \boldsymbol{x}_R$. The RSR frame rotates at approximately 1 deg/day with respect to the ECI frame, due largely to the annual motion of the Earth (and L_2) about the sun, modified by the motion of

Presented as Papers 2002-4578 and 2002-4580 at the Guidance, Navigation, and Control Conference, Monterey, CA, 5–8 August 2002; received 21 November 2003, revision received 22 March 2004; accepted for publication 23 March 2004.

*Aerospace Engineer, Guidance, Navigation, and Control Systems Engineering Branch. Fellow AIAA.
†Aerospace Engineer, Flight Dynamics Analysis Branch.
‡Associate Branch Head, Flight Dynamics Analysis Branch. Senior Member AIAA.
§Aerospace Engineer, Space Systems Mission Branch.

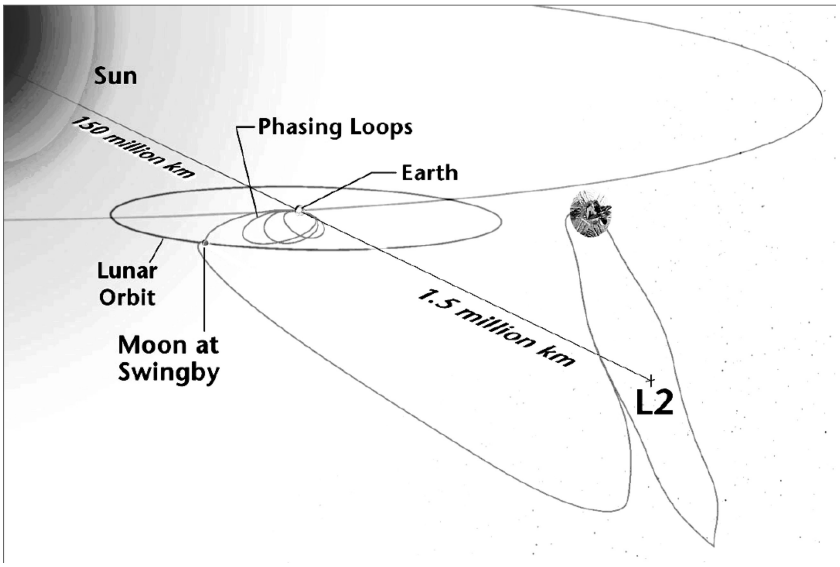

Fig. 1 WMAP trajectory to L_2.

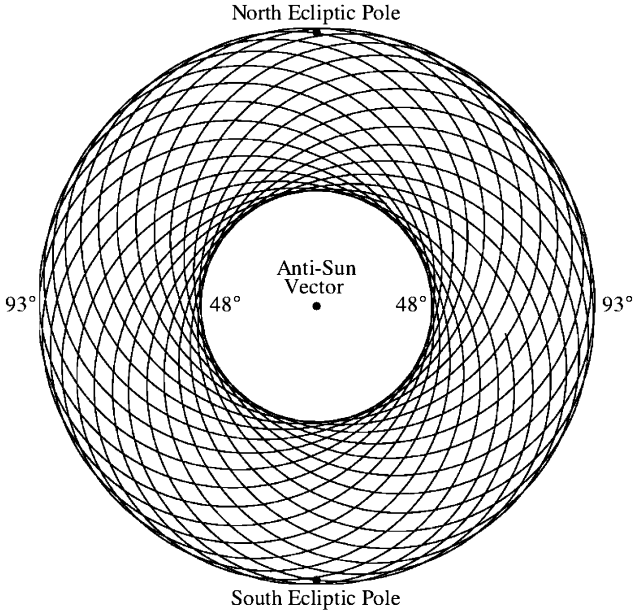

Fig. 2 WMAP scan pattern.

WMAP in its Lissajous orbit around L_2. The body frame is centered at the spacecraft center of mass with $\boldsymbol{z}_B$ axis parallel to the spacecraft centerline, directed from the instrument to the solar arrays, $\boldsymbol{y}_B$ axis normal to the instrument radiator faces, and $\boldsymbol{x}_B = \boldsymbol{y}_B \times \boldsymbol{z}_B$, as shown in Fig. 4. After initial attitude acquisition, the WMAP ACS always maintains the spacecraft $\boldsymbol{z}_B$ axis within 25 deg of the sun to satisfy thermal and power constraints, except during phasing loop orbit maneuvers. During the observing spin–scan motion, the $\boldsymbol{z}_B$ axis is maintained at the more precise angle of 22.50 ± 0.25 deg of the sun to satisfy milli-Kelvin-level thermal stability requirements.

The tight cost and weight restrictions imposed on a MIDEX spacecraft led to the WMAP ACS architecture shown in Fig. 5. This is basically single string, with limited redundancy in carefully selected areas. The attitude is sensed by an inertial reference unit (IRU), 2 star trackers, a digital sun sensor (DSS), and 12 coarse sun sensors (CSSs); it is controlled by three reaction wheel assemblies (RWAs) and a propulsion system. The ACS flight software resides in two redundant sets of microprocessors and electronics. Each set includes a main spacecraft processor (Mongoose V) and an attitude control electronics remote services node (ACE RSN), and each Mongoose V can communicate with either ACE RSN. With the exception of the CSSs, all of the attitude sensors and actuators communicate with both sides of the electronics. WMAP has neither magnetometers nor magnetic torquers because the ambient magnetic field at L_2 is too uncertain to serve as a reference and too small to provide magnetic torques, the smallness being one of the reasons for choosing the L_2 orbit. More detail on the WMAP ACS hardware suite may be found in Refs. 16, 18, and 19.

The IRU comprises two Kearfott two-axis rate assemblies (TARAs), one with input axes aligned with the $\boldsymbol{z}_B$ and $\boldsymbol{x}_B$ axes and the other with input axes aligned with the $\boldsymbol{z}_B$ and $\boldsymbol{y}_B$ axes. This gives redundant rate inputs on the $\boldsymbol{z}_B$ axis; the DSS outputs can be differentiated to provide the rate on one of the other axes in the event of a single TARA failure. This gives noisier rate data, but still meets spacecraft pointing requirements.

Lockheed Martin autonomous star trackers (ASTs)[18] were selected for their capability to acquire and track stars autonomously at the WMAP scan rate. The boresights of the two ASTs are in the $\pm\boldsymbol{y}_B$ directions. Each AST tracks up to 50 stars simultaneously in its 8.8-deg square FOV, matches them to stars in an internal star catalog, and computes its attitude as an ECI-referenced quaternion with accuracy of 21 arc-s (1σ) around its boresight axis and 2.3 arc-s (1σ) in the other two axes. The ACS uses only one AST; the other provides redundancy.

The Adcole two-axis DSS has two heads, each with 64-deg square FOV and an accuracy of 1 arc-min (3σ). The centers of the FOV of the two heads are in the $\boldsymbol{x}_B$–$\boldsymbol{z}_B$ plane at angles of ± 29.5 deg from the $\boldsymbol{z}_B$ axis. The CSSs are cosine eyes located in pairs looking outward from the edges of the six solar array panels, with one eye in each pair wired to the primary ACE RSN and the other to the backup ACE RSN. The pairs point alternately 36.9-deg up and 36.9-deg down from the $\boldsymbol{x}_B$–$\boldsymbol{y}_B$ plane, providing full 4π sr coverage.

The RWAs are Ithaco type-E wheels, each with a momentum storage capacity of 70 N · m · s. As already discussed, the angular momentum of the RWAs counterbalances the body's spin angular momentum to maintain the total system angular momentum near zero while executing the spin–scan observing motion. The available reaction torque of each wheel is 0.35 N · m, but this is limited to 0.215 N · m by the WMAP software to satisfy power constraints. The reaction wheel rotation axes are tilted 60 deg from the $-\boldsymbol{z}_B$ axis and uniformly distributed 120 deg apart in azimuth about this axis. With these orientations, the stored angular momentum biases all of the wheel speeds away from zero, avoiding zero-speed crossings that would occur if the wheel spin axes were oriented along the spacecraft body frame coordinate axes.

The propulsion system comprises eight monopropellant hydrazine reaction engine modules (REMs) and associated hardware. Each REM generates a maximum thrust of 4.45 N.

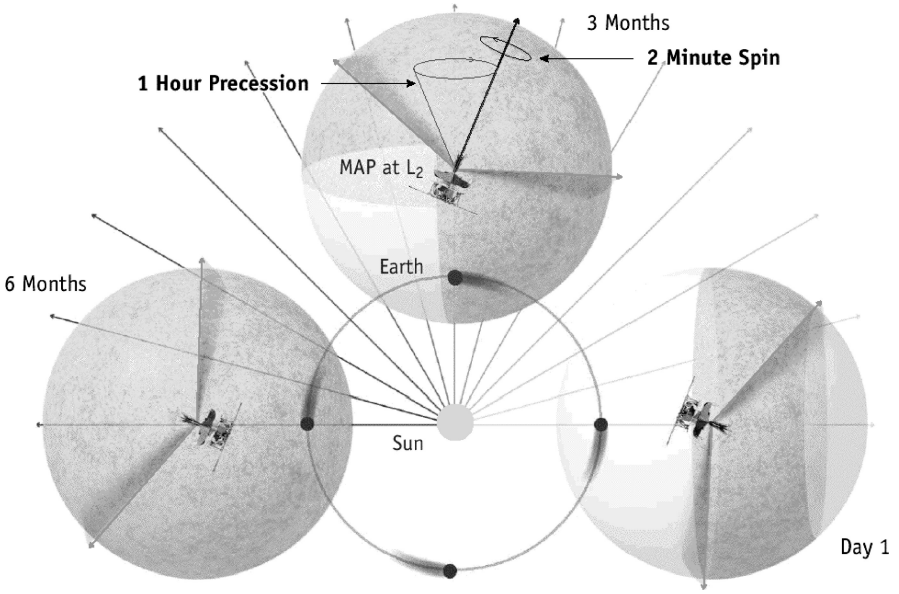

Fig. 3 WMAP spin–scan concept.

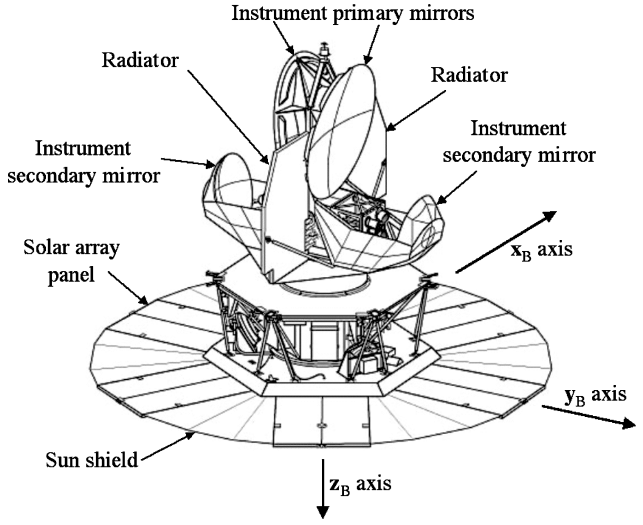

Fig. 4 Spacecraft layout.

Alternative ACS designs with fewer or no reaction wheels were considered, but it was difficult or impossible to provide either the desired spin–scan observing mode or a robust safehold mode with any of these designs. They also required frequent propulsive maneuvers to maintain the 22.50 ± 0.25 deg angle between the z_B axis and the sun and even to provide the spin–scan motion for designs without wheels. The resulting risk, thermal disturbances, and attitude perturbations were regarded as unacceptable, leading to the choice of the zero-momentum three-wheel design. A two-wheel backup mode was developed to provide reduced performance in the unlikely event of a reaction wheel failure, which has not occurred.[20]

Momentum Management Strategy

The propulsion system that carries out orbit maneuvers and stationkeeping also unloads accumulated system angular momentum during these maneuvers. Orbit maneuvers occur several times in the phasing loops, but stationkeeping is performed no more frequently than once every three months at L_2 to minimize interruptions of science observations. Each RWA can store 70 $\mathrm{N \cdot m \cdot s}$ of angular momentum, and so WMAP has ample momentum storage capacity on all axes in non-spinning modes and on the z_B axis while spinning about this axis. While executing the observing mode spin–scan, however, the system angular momentum that is slowly varying in the ECI frame rotates in the x_B–y_B plane at the fast spin rate. To avoid undesirable body motion, this momentum must be cycled among the three RWAs, absorbing some portion of their torque capability. As a result, the transverse momentum stored in the x_B–y_B plane cannot exceed 3 $\mathrm{N \cdot m \cdot s}$ in observing mode without adversely affecting attitude control.

Gravity gradient, atmospheric drag, and outgassing torques are significant in the phasing loops, but the accumulated angular momentum of less than 1 $\mathrm{N \cdot m \cdot s}$ per orbit is easily stored until removal during orbit maneuvers at apogee or perigee. Solar radiation pressure torque is the only significant disturbance torque at L_2, and the rotation about the spin axis reduces its average along the x_B and y_B axes by more than two orders of magnitude compared to its instantaneous value. The only potentially troublesome component is a pinwheel torque along the z_B axis, which might result from an imperfect deployment of the solar array panels. The angular momentum is accumulated in inertial space, so that it is clear from Fig. 3 that the pinwheel torque at one point in the orbit leads to a transverse angular momentum three months later. This means that any accumulation of angular momentum from the pinwheel torque of more than about 0.03 $\mathrm{N \cdot m \cdot s}$ per day would require momentum unloading more frequently than desired.

Preflight estimates of the pinwheel torque gave angular momentum accumulation ranging from 0.0016 to 0.065 $\mathrm{N \cdot m \cdot s}$ per day, depending on the accuracy of deployment of the solar arrays and the resulting symmetry of the spacecraft.[14] The worst-case estimate would reach the observing mode system angular momentum limit of 3 $\mathrm{N \cdot m \cdot s}$ in 46 days, which is highly undesirable. Providing movable tabs to be adjusted to minimize solar torques was considered and rejected from a desire to avoid moving mechanisms wherever possible, and the solar array deployment mechanisms were carefully designed and constructed to avoid unacceptable solar torques. Flight data indicates an angular momentum accumulation of about 0.006 $\mathrm{N \cdot m \cdot s}$ per day, which easily meets the three-month requirement. In fact, because this is less than 0.03 $\mathrm{N \cdot m \cdot s}$ per day, Fig. 3 shows that the pinwheel torque will begin to unload the accumulated angular momentum in the next three months, so that no unloading by the REMs is required at all, in principle. Because the orbit perturbations at L_2 have been well within expectations, it has been possible to perform stationkeeping and momentum unloading only once every four months, rather than every three months.

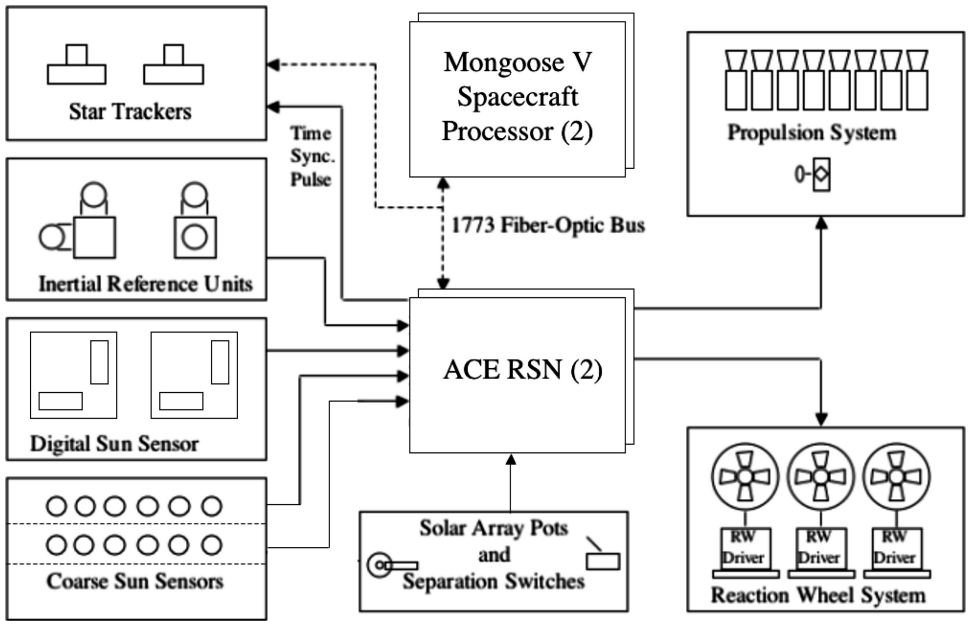

Fig. 5 ACS architecture.

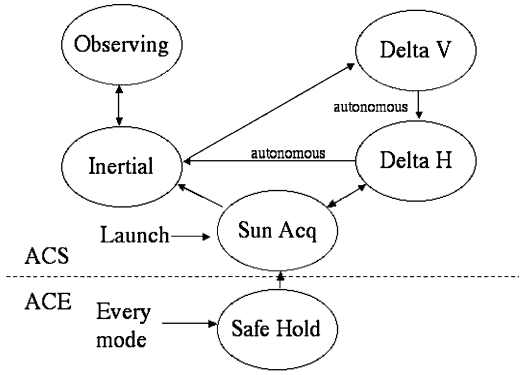

Fig. 6 ACS mode transitions.

ACS Operational Modes

WMAP has six ACS modes, which are all executed at a 1-Hz rate. The sun acquisition, inertial, observing, delta V, and delta H modes are implemented in the Mongoose V, whereas the safehold mode resides in the ACE RSN. Figure 6 shows the modes and the transitions among them. Anomalous behavior can result in autonomous transitions from any other mode to sun acquisition mode or safehold mode, even though these transitions are not shown explicitly. Each mode will be discussed later, including a discussion of the sensors, actuators, and control algorithms used in that mode. Examples of in-flight performance are also provided.

ACS Design and Performance

Sun Acquisition Mode

Sun acquisition mode uses the CSS, IRU, and RWAs to acquire and maintain a thermally safe and power-positive orientation with the spacecraft z_B axis within 25 deg of the sun, starting from any initial orientation and with any initial body momentum less than [13, 13, 55] N · m · s. This is the mode entered after separation from the launch vehicle. If the rates at entry to the RWA-based sun acquisition mode exceed those that can be handled by this mode, the REM-based delta H mode can be commanded to reduce the rates to an acceptable level, after which the spacecraft returns to sun acquisition mode. Transition from sun acquisition mode to inertial mode can be commanded after the sun has been acquired and the attitude has been initialized using star tracker data. Transition to the Mongoose control modes from the ACE safehold mode is through sun acquisition mode. Normal exit from sun acquisition mode is to either delta H or inertial mode, depending on the residual spacecraft spin rate.

The attitude error signals in sun acquisition mode are calculated by computing the cross product of the sun vector computed from CSS measurements with the desired sun vector. The nominal desired sun vector points the $+z_B$ axis, the solar array normal, directly at the sun. The attitude error signals are limited and multiplied by a proportional control gain. The rate error signal is the body rate measured by the IRUs. The rate error vector is multiplied by the spacecraft inertia and then each axis is multiplied by a derivative control gain. The output of this proportional–derivative (PD) control algorithm is three torque commands in the body frame. A body-to-wheel reference frame transformation matrix is used to transform these commands to the reaction wheel frame. The wheel torque commands are scaled down by a common factor if the largest command exceeds the wheel torque capability, so that the torque direction is preserved while the largest command is the maximum reaction wheel torque command.

The sun acquisition mode was subjected to extensive prelaunch analysis and high-fidelity simulations with a wide range of entry conditions and was found to meet its performance requirements for all initial system momentum magnitudes of 55 N · m · s or less. Because this level represented 2σ separation rates from the Delta II third stage, a contingency thruster momentum unload was unlikely but possible. In addition, there were a few degenerate cases, for example, 180 deg off of the Sun with zero rates, that did not satisfy the requirements, but these were deemed too unrealistic to be of concern.

Performance on orbit agreed with the prelaunch simulations. After an expected postlaunch communications gap, contact was established with WMAP via the tracking and data relay satellite TDRS-W at 21:03 Greenwich Mean Time (GMT), 77 min after launch and 10 min before spacecraft separation. At the beginning of this contact, WMAP was still in the Delta II third-stage spin; gyro rates were saturated (over 5.3 deg/s), and the system momentum magnitude measurement was over 90 N · m · s, as shown in Fig. 7. At 21:13 GMT, the Delta II yo-yo despin mechanism was activated by a timer to remove most of the third-stage spin, after which WMAP separated from its booster. The first telemetry update, 16 s after despin, showed the gyros desaturated with all axes below 1 deg/s and the computed system momentum reduced to approximately 10 N · m · s. The solar arrays began to deploy 14 s after separation, and the spacecraft

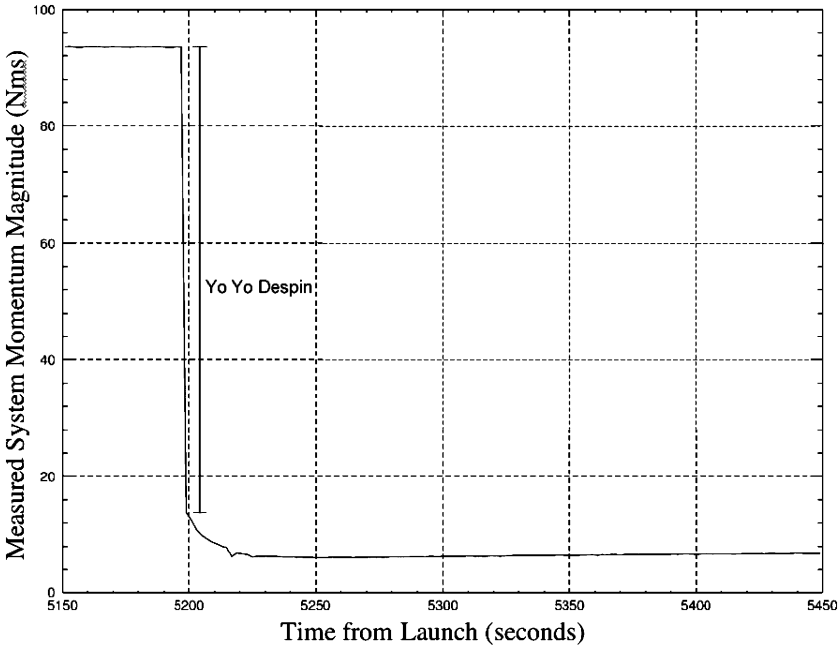

Fig. 7 System momentum magnitude at separation.

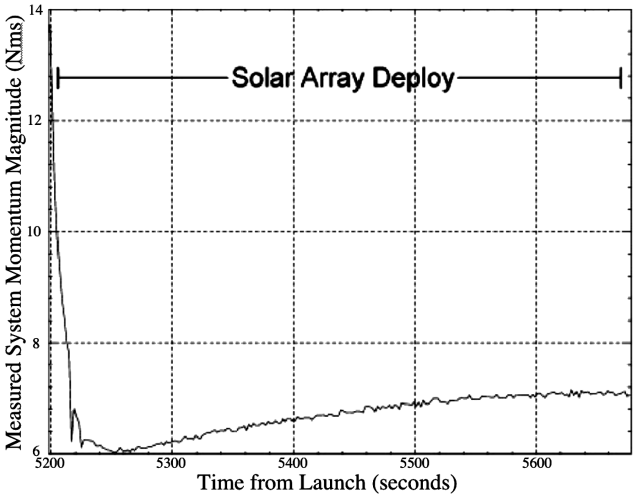

Fig. 8 System momentum magnitude at solar array deployment.

reported that all arrays were deployed to within 25 deg of their fully deployed state 8 s later. Figure 8 shows the apparent change in the system momentum magnitude as the mass properties of the spacecraft changed during array deployment and fuel spin down. The actual system momentum is constant after separation, but the onboard computation uses a rigid-body model with constant moments of inertia, which is not an accurate representation of reality before solar array deployment. The arrays opened fully in 4 min, at which point the system momentum magnitude was 7 $\mathrm{N}\cdot\mathrm{m}\cdot\mathrm{s}$, well within the maximum level of 55 $\mathrm{N}\cdot\mathrm{m}\cdot\mathrm{s}$ at which sun acquisition mode could acquire the sun. Figure 9 shows the CSS and DSS measured sun angles at separation. Note that the sun was out of the DSS FOV until 5530 s of the plot. The spacecraft acquired the sun within 7 min of separation. The spacecraft was declared safe on the sun at 21:26 GMT, 13 min after separation.

In the design of the failure detection and correction logic for WMAP, sun acquisition mode was used in many cases as a first level of safing in the event of a problem. Fortunately, there were no on-orbit anomalies that caused an autonomous entrance into sun acquisition mode. During the first week of the launch and in-orbit checkout period, sun acquisition mode was used as the base mode for the spacecraft when other operations were not being conducted. Once observing mode was checked out, it or inertial mode became the base mode. The maneuver plan used for each of the calibration maneuvers at apogee and orbit maneuvers at perigee commanded the spacecraft into sun acquisition immediately after each maneuver. In all cases, the mode satisfied all of its requirements.

Inertial Mode

Inertial mode acts as a staging mode between the other operations of the spacecraft; all Mongoose modes other than delta V have the capability to enter this mode. Inertial mode can either hold the spacecraft in an inertially fixed orientation or slew the spacecraft between two different orientations. This is an RWA- and IRU-based mode, with DSS and AST measurements used in an onboard extended Kalman filter to update the gyro bias and quaternion error estimates. Normal exits from inertial mode are by ground command only. The basic requirements for inertial mode are to acquire and hold a fixed target quaternion within 10 min and to maintain the spacecraft z_B axis within 25 deg of the sunline at all times. The desired orientation is commanded as a desired ECI-to-body quaternion q_c. (Refs. 21 and 22). A slew will be executed if the commanded quaternion is not close to the current spacecraft orientation. The attitude is controlled by RWA torques computed from attitude and rate errors in a PD controller.

The attitude errors are expressed as twice the vector part $\boldsymbol{q}_e$ of an error quaternion, which is the quotient of the commanded quaternion and an estimated quaternion $\hat{q}$:

$$q_e = \pm q_c \otimes \hat{q}^{-1} \tag{1}$$

In this and in the following equations, we use the quaternion product convention of Refs. 22 and 23 rather than that of Ref. 21 so that the order of quaternion multiplication is the same as that of the corresponding direction cosine matrices. The sign in Eq. (1) is chosen to assign a positive sign to the scalar component of q_e, which has magnitude close to unity for small pointing errors. The small-angle approximation is used at all times for the attitude error; this introduces inaccuracies for large slews, but does not affect the performance of the controller, and because there is no direction preference for the slews, it is not a problem.

The estimated quaternion is computed by the Kalman filter, with IRU, AST, and DSS measurements as input (see Refs. 23–25). This is similar to Kalman filters employed on several previous Goddard

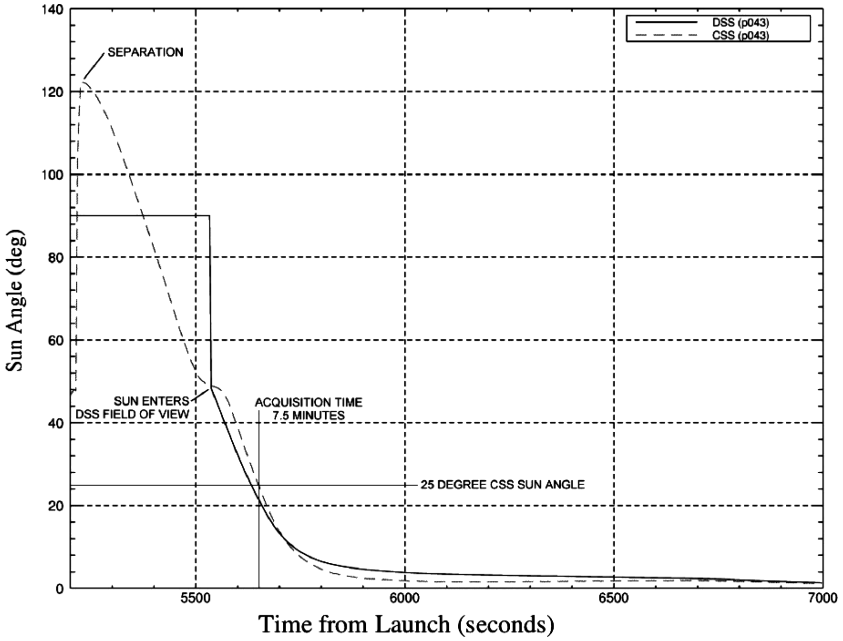

Fig. 9 Sun angles at separation.

Space Flight Center missions, except that the AST produces a measured attitude quaternion rather than observed star vectors.[18] This simplifies the ACS software computations by removing the burden of star identification and the responsibility for the onboard star catalog. The Kalman filter will be discussed in more detail later in this paper.

The onboard Kalman filter also estimates corrections to the gyro drift rates that are subtracted from the IRU-measured body rates to produce the body rate vector. Because the desired rates in the inertial mode are zero, the rate error vector $\boldsymbol{\omega}_e$ is the negative of the body rate vector measured by the IRU:

$$\boldsymbol{\omega}_e = -\boldsymbol{\omega}_{BI} \tag{2}$$

The commanded control torque in the body reference frame is given by[25–27]

$$\boldsymbol{T} = J[k_d\boldsymbol{\omega}_e + k_p(2\boldsymbol{q}_e)] \tag{3}$$

where

$$J = \begin{bmatrix} 600.28 & -3.57 & 0.17 \\ -3.57 & 611.44 & 0.25 \\ 0.17 & 0.25 & 507.90 \end{bmatrix} \tag{4}$$

is the WMAP moment of inertia tensor in SI units and k_d and k_p are the derivative and proportional gains, respectively. The factor of two multiplying the error quaternion reflects that the quaternion errors are one-half the angle errors in the small-angle approximation. The controller outputs are the same type of torque commands as described in the Sun Acquisition Mode section and are sent to the RWAs in the same manner.

A dynamic attitude limiter is employed in the inertial mode to enable the spacecraft to meet the 25-deg sun constraint during large slews. Before the limiter was implemented, the sun angle grew as large as 38 deg in simulated 45-deg inertial mode slews with high spin errors in the z_B axis. With the limiter implemented, the angular velocity rapidly approaches the steady-state value

$$\boldsymbol{\omega}_{BI} = (k_p/k_d)(2\boldsymbol{q}_e)_{\text{lim}} \tag{5}$$

when the attitude errors exceed their limiting values. The dynamic attitude error limiter calculates attitude error limits on the three axes that preserve the direction of the resulting slew and prevent the spacecraft from violating the sun constraint for any slews with spin angles from 0 to 180 deg.

In addition to accepting ground-commanded attitudes, the inertial mode has two precomputed quaternions onboard. One will point the spacecraft $+z_B$ axis toward the sun, and the other will point the spacecraft $+z_B$ axis 22.5 deg from the sun. The commands have fixed quaternions relative to the RSR frame described previously. Inertial mode also accepts quaternions from a command quaternion table (CQT), which is a table of times and quaternions representing a particular attitude profile for the duration of the CQT. The CQT can be loaded with different quaternion sequences and was used to command the gyro calibration slew profile as part of the in-orbit checkout. The CQT was also used to command the spacecraft to the proper orbit maneuver orientations and to command the spacecraft to hold the thrust direction parallel to the velocity vector before, during, and after the maneuvers.

WMAP was in the inertial mode for a long period of time during the first week of the mission, leading to one surprise: Inertial mode does not hold the spacecraft in an inertially fixed orientation. When the spacecraft was commanded to point at the current sun location (via the precomputed sun-pointing command discussed earlier), the sunline angle from the spacecraft z_B axis was expected to change by about 1 deg/day, consistent with the spacecraft's motion relative to the sun. Instead, the spacecraft telemetry showed that the spacecraft maintained a sun-pointing attitude. The difference between the estimated quaternion and the command quaternion slowly climbed at approximately 1 deg/day and was reset to zero whenever we commanded a sun-pointing attitude, as expected. However, the telemetered attitude errors and sun angles did not reflect this.

Inspection of the flight code and ACS simulation code revealed that the portion of the simulation used to generate flight software automatically only understands commands and attitudes in the RSR frame. When a new inertial (ECI) quaternion is commanded, the flight software converts it to an RSR reference frame quaternion before handing it off to the controller. The controller computes the commanded inertial quaternion once per second as the product of this RSR-to-body quaternion and an ECI-to-RSR quaternion:

$$q_c = q_{BI} = q_{BR} \otimes q_{RI} \tag{6}$$

The ECI-to-RSR quaternion is computed once per minute from onboard ephemeris models, which are updated at the same rate. If the

conversion of the ECI command quaternion to an RSR quaternion were done each time the controller was entered, that is, once per second, or when the ephemeris was updated, then the command quaternion within the inertial mode controller would remain inertially fixed. However, this conversion is only done with the initial command, so that the controller continues to control to the static RSR frame quaternion. As the ephemeris updates and the RSR frame moves, the controller moves with the RSR frame. Thus, commanding a sun-pointing attitude results in the inertial mode controller continuing to follow the sun. This was not discovered in testing primarily because the longest stay in inertial mode in a simulation run, build test, or acceptance test was an hour or less, so the effect was too small to be seen in the test data. It was important to understand the source of this unintended behavior, but it was not corrected because it actually proved to be helpful in practice.

Observing Mode

The observing mode used for science observations is an an RWA- and IRU-based mode, with the same Kalman filter employing DSS and AST measurements as in the inertial mode. The RWAs provide the angular momentum that preserves a near-zero system momentum and the torques that maintain both the 22.5-deg angle between the spin axis and the sunline and the desired sky-scan rates shown in Fig. 2. The tolerance on both rates is 5%, and the tolerance on the sunline angle is 0.25 deg. The observing mode differs from the inertial mode in that the commanded quaternion is time varying, the commanded rates are nonzero, and both a commanded angular acceleration and a commanded gyroscopic torque are used in a feedforward loop to eliminate attitude hangoff. The attitude error is computed as in inertial mode, but the commanded attitude quaternion comes from the desired motion relative to the sunline, rather than being fixed. Normal transitions into or out of the observing mode are via the inertial mode.

The RSR-to-body attitude providing the desired spin–scan attitude motion is more conveniently expressed in terms of 3–1–3 Euler angles[21,22] than in terms of a quaternion. The Euler angle rates that give the desired scan rates are

$$\dot{\phi}_c = -1 \text{ revolution/h} = -0.001745 \text{ rad/s}, \qquad \dot{\theta}_c = 0$$

$$\dot{\psi}_c = 0.464 \text{ rpm} = 0.04859 \text{ rad/s} \tag{7}$$

These Euler angle rates are modified so that a large rate command change when entering or exiting the observing mode will not cause the spacecraft to violate the sunline constraint. If the rate error in the PD controller were too large, then the rate path would saturate the wheel command, and no attitude error signal would get into the control torque, resulting in an uncontrolled spacecraft attitude. To avoid this, the input Euler angle rates are differenced with the previous modified rates, limited to 2.5×10^{-4} rad/s^2, and then integrated to get new modified rates. The result is a steady change in the amount of the input rates fed into the control system, which generates a spin-up when entering the observing mode and a spin-down when exiting. This effect is seen in Fig. 10, which shows the initial slew from the z_B axis on the sunline to the 22.5-deg sunline angle (starting just after 1000 s), and then the spin-up into the compound spin (starting at about 1600 s). The limiter has no effect once the compound spin has been established, because then the modified Euler rates attain the constant values given by Eq. (7).

The commanded values of the three Euler angles at the ith control cycle are given in terms of the modified Euler angle rates by

$$\phi_c(i) = \phi_c(i-1) + \dot{\phi}_c \Delta t, \qquad \theta_c(i) = 22.5 \text{ deg} = 0.3927 \text{ rad}$$

$$\psi_c(i) = \psi_c(i-1) + \dot{\psi}_c \Delta t \tag{8}$$

where $\phi_c(i-1)$ and $\psi_c(i-1)$ are the values from the previous cycle and Δt is the 1-s control cycle time. These 3–1–3 Euler angles are converted to the commanded RSR-to-body quaternion q_{BR} by the standard equations,[21,22] and the commanded inertial quaternion is computed as the product of an RSR-to-body and an ECI-to-RSR

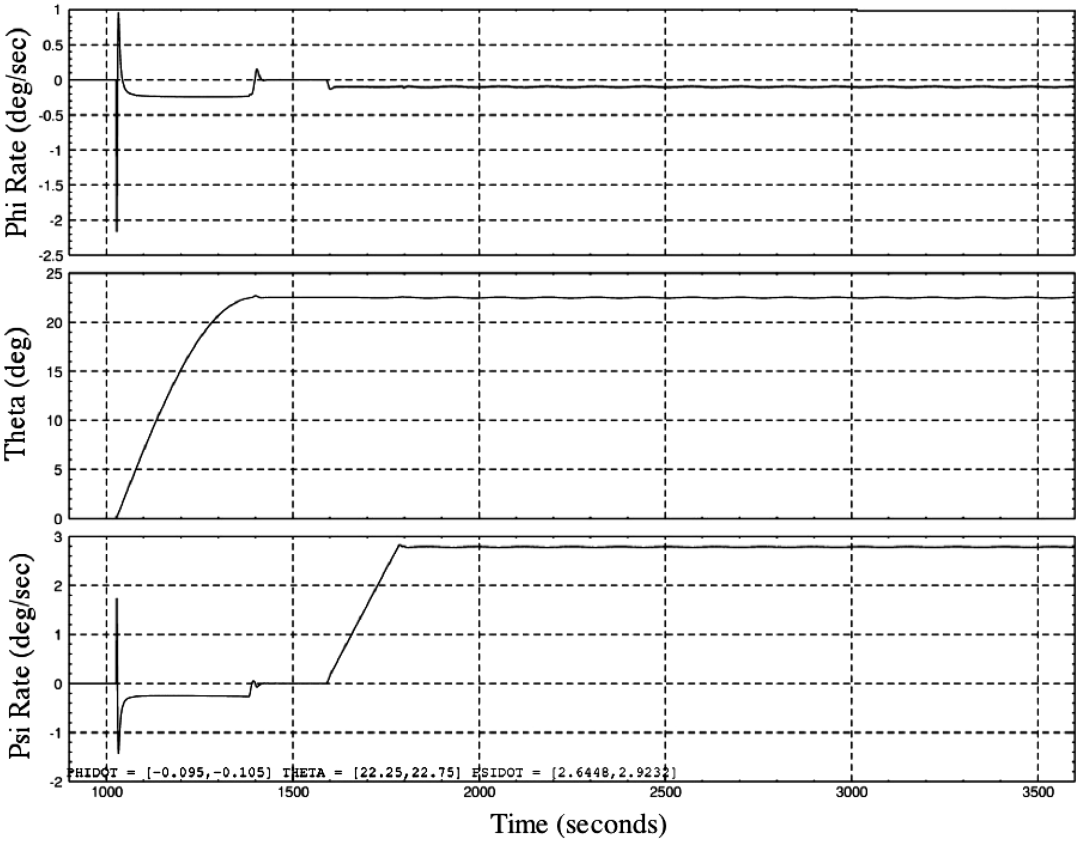

Fig. 10 Euler angles/rates entering observing mode.

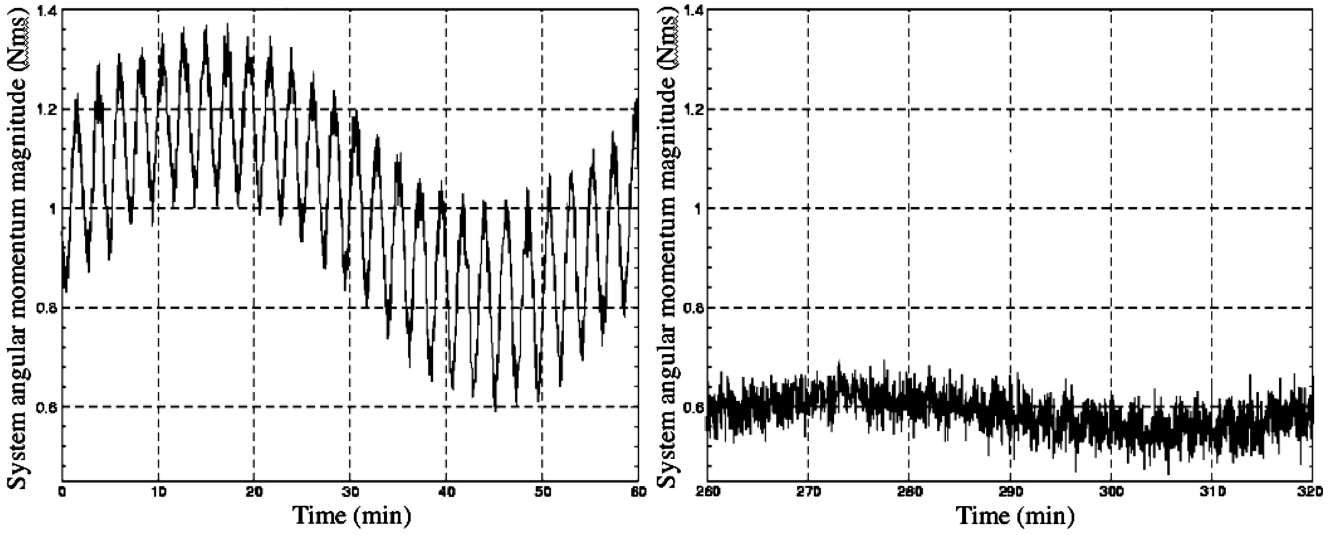

a) Precalibration **b) Postcalibration**

Fig. 11 Pre- and postcalibration system angular momentum magnitude.

quaternion as in the inertial mode. The error quaternion is computed as the quotient of the commanded and estimated quaternion, also as in the inertial mode.

The rate error vector $\boldsymbol{\omega}_e$ is the difference between a commanded body rate vector $\boldsymbol{\omega}_c$ and the body rate vector $\boldsymbol{\omega}_{BI}$ measured by the IRU:

$$\boldsymbol{\omega}_e = \boldsymbol{\omega}_c - \boldsymbol{\omega}_{BI} \tag{9}$$

The commanded body rate vector $\boldsymbol{\omega}_c$ is computed from the commanded Euler angles and rates by the standard equation[21,22]

$$\boldsymbol{\omega}_c = \begin{bmatrix} \sin\theta_c \sin\psi_c & \cos\psi_c & 0 \\ \sin\theta_c \cos\psi_c & -\sin\psi_c & 0 \\ \cos\theta_c & 0 & 1 \end{bmatrix} \begin{bmatrix} \dot{\phi}_c \\ \dot{\theta}_c \\ \dot{\psi}_c \end{bmatrix} \tag{10}$$

One of the feedforward terms, the angular acceleration needed to follow the commanded attitude and rates, is derived by differentiating the equation for $\boldsymbol{\omega}_c$ with respect to time. Because the feedforward acceleration is only important during the compound spin, we can compute the derivative assuming that $\dot{\phi}_c$, $\dot{\psi}_c$, and θ_c are all constant, giving

$$\dot{\boldsymbol{\omega}}_c = \dot{\psi}_c \dot{\phi}_c \sin\theta_c \begin{bmatrix} \cos\psi_c \\ -\sin\psi_c \\ 0 \end{bmatrix} \tag{11}$$

This acceleration is multiplied by the spacecraft inertia to get a commanded torque.

The second feedforward torque is the gyroscopic feedforward torque, used to move the system momentum around among the reaction wheels as required by its constancy in inertial space:

$$\boldsymbol{T}_g = \boldsymbol{\omega}_c \times \boldsymbol{H}_{\text{sys}} \tag{12}$$

These feedforward torques are added to the output of the PD controller to generate the complete control torque for the RWAs:

$$\boldsymbol{T} = J[k_d \boldsymbol{\omega}_e + k_p(2\boldsymbol{q}_e) + \dot{\boldsymbol{\omega}}_c] + \boldsymbol{T}_g \tag{13}$$

This control torque is in the body frame and is sent to the RWAs in the same manner as in the other modes.

Initially, the precession rate $\dot{\phi}$ in the observing mode did not meet its 5% accuracy requirement, showing a 7% variation at the spin period. This was attributed to an inaccurate value of system momentum in the gyroscopic feedforward loop arising from a scale factor error in the RWA tachometer signals. Evidence for this was that the magnitude of the system momentum, which should be constant, had a 0.4 N · m · s oscillation at spin period and increased during spin-up by 1.0 N · m · s. Comparing a high-fidelity simulation with flight data determined that changing the tachometer scale factors by about 2.5% for RWA1 and about 4% for RWA2 and RWA3 could remove the oscillation and spin-up offset. Loading these new scale factors dramatically reduced the variation of the precession rate as well as the spin-period oscillation and the spin-up offset in the computed system momentum magnitude, which are shown in Fig. 11. A recent analysis is in basic agreement with these results.[28]

Once all sensors and actuators were calibrated, the observing mode met the 5% requirement on the commanded Euler rates and the 0.25-deg sun angle control requirement, as shown in Fig. 12 and the nearly perfect circle described by the DSS data in the body frame shown in Fig. 13.

Delta *V* Mode

Delta V mode, which uses the REMs to adjust the orbit in either the initial phasing loops or for L_2 stationkeeping, is only entered from the inertial mode. A command sequence specifies maneuver duration, direction, and start time. The desired attitude in terms of either a single quaternion or a CQT can be configured either via command or by table load. The desired set of thrusters to be used is specified via command. The spacecraft remains in the inertial mode to slew from the initial orientation to the desired attitude for the start of the maneuver and transitions to delta V mode at the requested start time. The only sensors used in delta V mode are the IRU and RWA tachometers. This mode uses a PD controller to hold the spacecraft to a commanded quaternion attitude while executing the maneuver. The output of the controller is transformed into thruster-firing commands using a pulse width modulator with a minimum pulse width of 0.04 s. Off-pulsing the primary set of thrusters and on-pulsing the others holds the desired attitude. Normal exit is autonomously to the delta H mode.

Anomalous spacecraft motion experienced during some early maneuvers was later attributed to torques caused by the evaporation of ice condensed on the back of the solar arrays and sun shields.[29] Despite this unexpected phenomenon, maximum pointing errors during the nine delta V maneuvers performed in the first three months of the mission were smaller than predicted (3.7 vs 5.5 deg), and the imparted velocity increments were accurate to 1%. Less than 15 kg of hydrazine propulsion fuel was expended to get to L_2, about one-half the amount budgeted for this phase of the mission. The 57 kg of fuel remaining for stationkeeping and momentum unloading at L_2 will easily support a four-year extended mission.

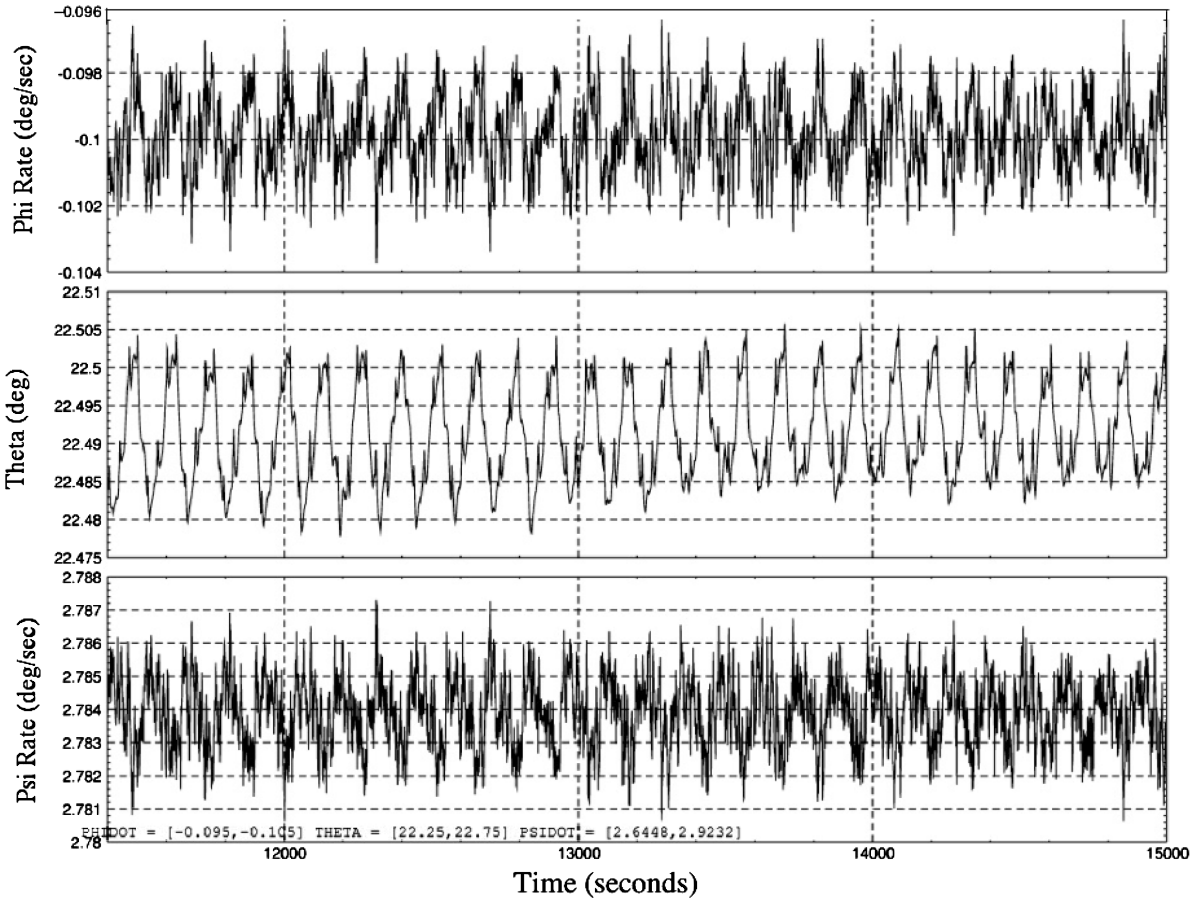

Fig. 12 Postcalibration observing mode performance.

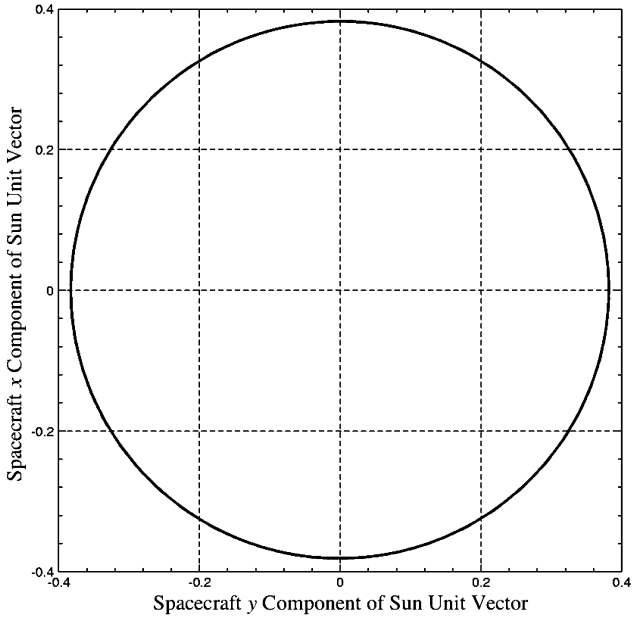

Fig. 13 DSS measurements in observing mode.

Delta *H* Mode

Delta H mode uses the REMs to unload spacecraft system angular momentum, which is computed using the RWA tachometers and IRU. It is entered autonomously on exit from the delta V mode and can be commanded from the inertial or sun acquisition mode if necessary. If entry was from the delta V or inertial mode, the ACS autonomously transitions to the inertial mode after the momentum has been reduced to less than $0.3\ \mathrm{N \cdot m \cdot s}$. If the delta H mode was entered from the sun acquisition mode, the autonomous exit upon completion of the momentum unloading is back to the sun acquisition mode. The delta H mode uses the same pulse width modulator as delta V, with the exception that all thrusters are operated in an on-pulsing manner for delta H.

As was stated earlier, the delta H mode could have been commanded immediately after separation from the launch vehicle if the tipoff angular momentum had exceeded the capacity of the RWAs. This was neither expected nor required, and so commanding the delta H mode from the sun acquisition mode was delayed until $4\frac{1}{2}$ h after separation, at which time it required only 6 s to remove the $7\ \mathrm{N \cdot m \cdot s}$ of tipoff angular momentum shown in Fig. 8.

Safehold Mode

The safehold mode is implemented in the ACE RSN, and so it can be entered autonomously in the event of a Mongoose anomaly. It has two configurations, which differ by the rate information used. The first, safehold/IRU, is a near copy of the sun acquisition mode in the Mongoose. The second, safehold/CSS, is a minimum-hardware mode using only the RWAs and CSSs, with rate errors computed by numerically differentiating the position error signals. Because it lacks z_B-axis rate information from the gyros, safehold/CSS cannot tolerate as much system momentum as can the sun acquisition or safehold/IRU mode. Because the CSSs are insensitive to rotations about the sunline, antirunaway compensation is applied to prevent uncontrolled spinning about the satellite's z_B axis. Applying equal torques to the three wheels if the sum of their speeds exceeds a preset value suppresses z_B-axis rotation without applying a net torque in the x_B–y_B plane, thereby avoiding runaway. Exit from either safehold mode is by ground command only.

Charged particle flux from extreme solar activity on 5 November 2001 caused a power-on reset of the Mongoose processor. The ACS

transitioned autonomously to the safehold mode in the ACE RSN, which functioned exactly as designed to keep WMAP safe. The operations staff discovered the transition to safehold mode at the next telemetry pass about 12 h later, and recovery to observing mode was accomplished within 3 h of this discovery. Recovery from a similar safemode entry on 11 August 2003 was equally successful.

Attitude Determination Kalman Filter

Implementation and Operation

The WMAP Kalman filter is an extended Kalman filter that uses AST and DSS measurements to update the IRU-propagated attitude and to update the estimated IRU drift rate. The Kalman filter operates in sun acquisition and safehold modes, but the spacecraft does not use its output for attitude knowledge in those modes, which control the spacecraft based on an attitude calculated from the CSS measurements. The sun acquisition mode is, thus, ideal for observing the Kalman filter performance before using its output to control the spacecraft. With the ACS in observing mode during the phasing loops, stray light caused both ASTs to lose track when the moon was within a degree or so of the FOV, but only for a few seconds in a spin cycle, and only for three spin cycles in any precession cycle. No more than 13 AST readings were lost in any precession cycle. There is no moon, earth, or sun interference at L_2, and the ASTs have been routinely tracking 15 to 40 stars in the absence of interference.

The Kalman filter estimates a four-component quaternion and a three-component vector of gyro drift biases, but the attitude error covariance is in terms of small rotations between the truth and the estimate.[23–25] Thus, the covariance is a 6×6 matrix, with 3×3 submatrices,

$$P = \begin{bmatrix} P_{\text{attitude}} & P_{\text{correlation}} \\ P^T_{\text{correlation}} & P_{\text{drift bias}} \end{bmatrix} \tag{14}$$

The process noise covariance is also a 6×6 matrix, given by

$$Q = \begin{bmatrix} \left(\sigma_v^2 \Delta t + \frac{1}{3}\sigma_u^2 \Delta t^3\right) I_{3\times 3} & -\frac{1}{2}\sigma_u^2 \Delta t^2 I_{3\times 3} \\ -\frac{1}{2}\sigma_u^2 \Delta t^2 I_{3\times 3} & \sigma_u^2 \Delta t\, I_{3\times 3} \end{bmatrix} \tag{15}$$

where σ_v^2 is the intensity of the gyro rate white noise, σ_u^2 is the intensity of gyro rate random walk white noise, Δt is the propagation time, and $I_{3\times 3}$ is the 3×3 identity matrix. The first time the Kalman filter was enabled in the sun acquisition mode, parameters such as the measurement noise covariance matrix, the initial covariance matrix, and the residual tolerances were increased to launch values, because the sensors had not been calibrated in flight yet. The larger initial parameter values allowed the filter to converge and estimate attitude corrections and IRU bias, albeit at less accuracy than possible with a fully calibrated system. The initialization and nominal values of the parameters appear in Table 1.

During each control cycle, the IRU, DSS, and AST data are sampled at slightly different (but deterministic) times. The previous control cycle's estimated attitude quaternion is propagated to the current sample cycle time with a first-order propagator[21] using the IRU-measured rates, corrected with the previous cycle's gyro bias estimate. The attitude control is executed based on that propagated

Table 1 Kalman filter parameters

Noise parameter	Launch value	Nominal value
DSS measurement	0.5 deg	0.2 deg
AST measurement	120 arc-s	30 arc-s
Gyro rate random walk	0.01296 arc-s/s$^{3/2}$	0.001296 arc-s/s$^{3/2}$
Gyro rate white noise	7.2 arc-s/s$^{1/2}$	0.72 arc-s/s$^{1/2}$
Initial attitude covariance	(2 deg)^2 $I_{3\times 3}$	(0.5 deg)^2 $I_{3\times 3}$
Initial bias covariance	(40 deg/h)^2 $I_{3\times 3}$	(20 deg/h)^2 $I_{3\times 3}$

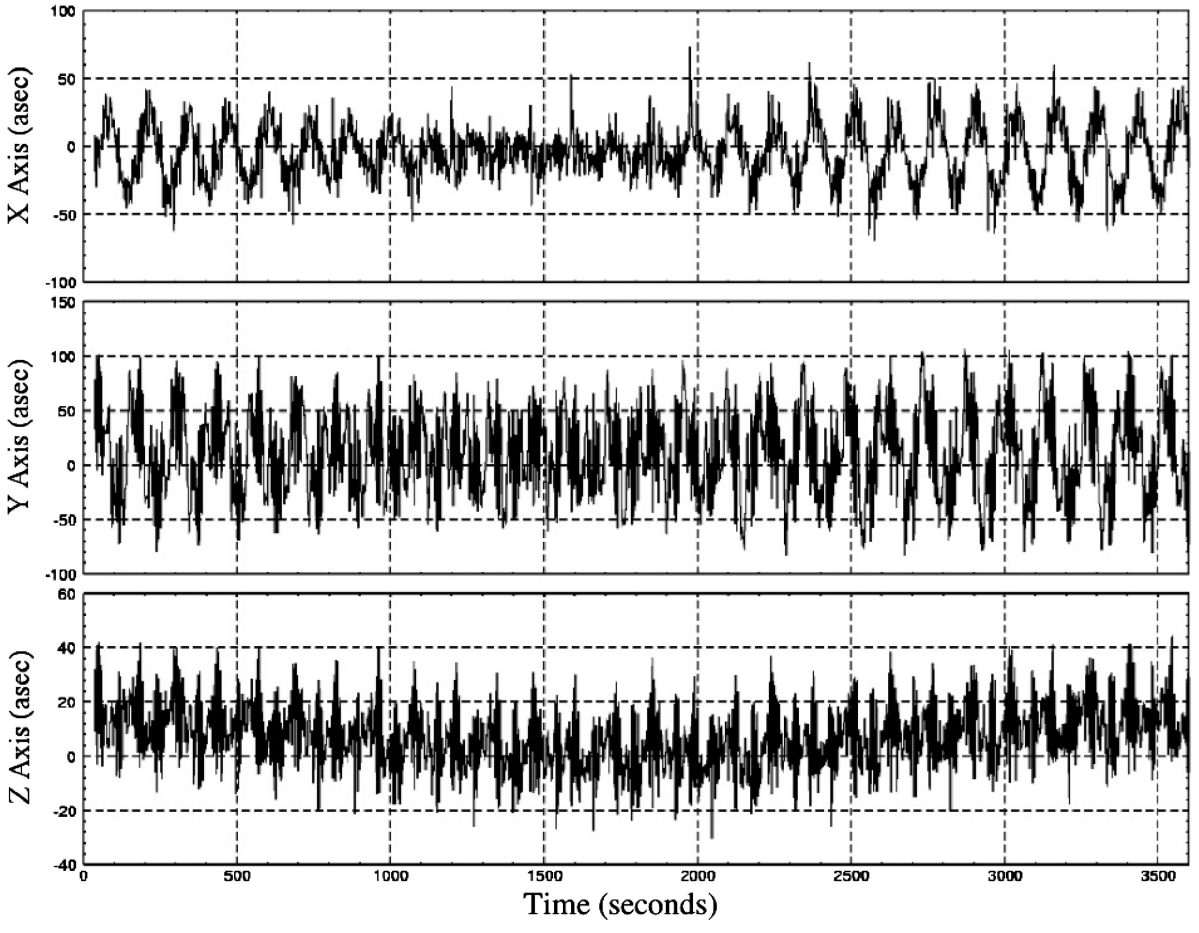

Fig. 14 DSS residuals.

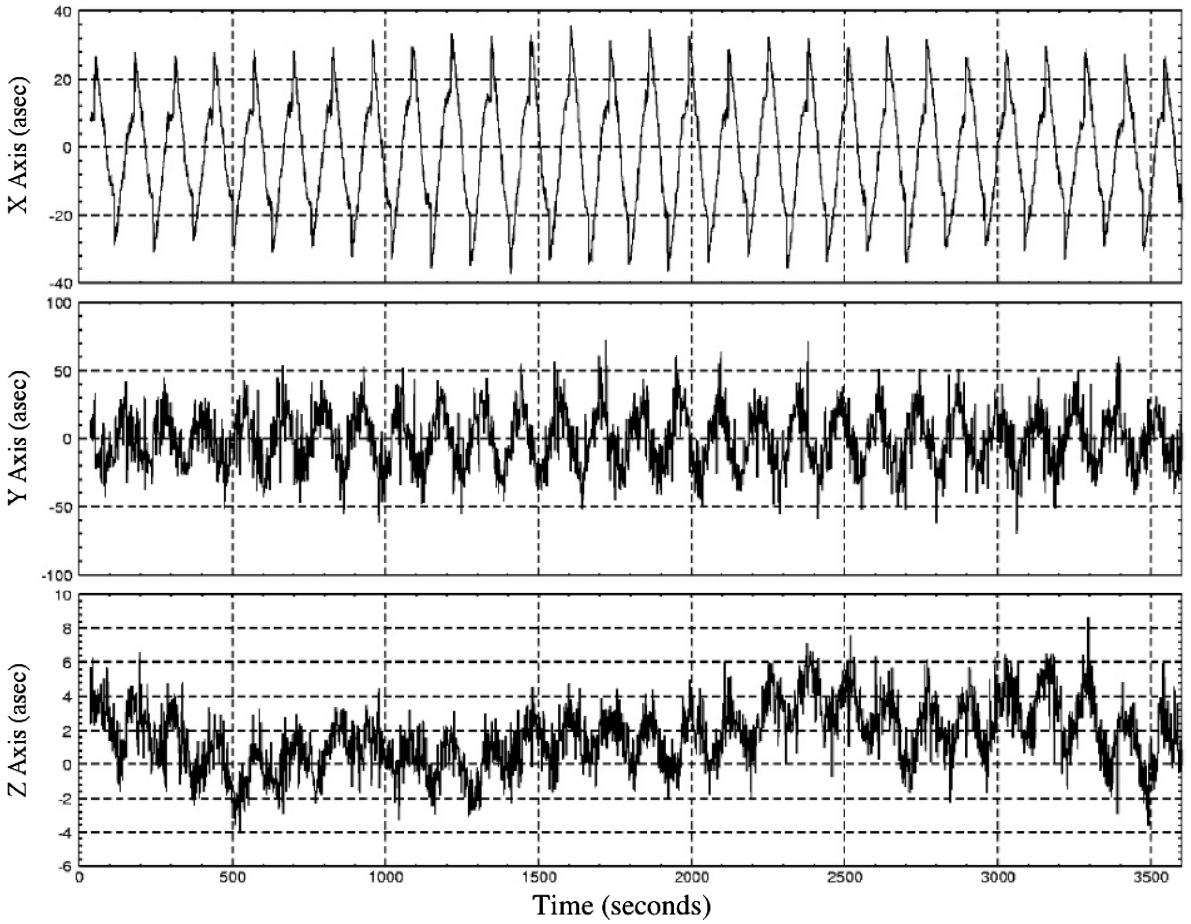

Fig. 15 AST residuals.

attitude and measured rate. The DSS and AST data are processed in the sensor data processing algorithms, and the resulting measurements (sun vector and attitude quaternion) are backpropagated to the IRU sample time with another first-order propagator, using the current body rate measurement. The backpropagation removes any attitude error that may result from the timing differences between the sensor samples, especially at the nominal observing mode spin rate. The Kalman filter uses the synchronized measurements to update the propagated quaternion, the estimated gyro drift bias, and the propagated covariance matrix.

Submodes within each control mode are used to determine whether or not the filter will update the attitude and gyro bias estimate. In general, if the control mode produces large accelerations on the body, the Kalman filter propagates the covariance matrix, but the estimated attitude and gyro bias are not updated. In inertial hold submode and observing scan/hold submode, the Kalman filter is used to update the estimates.

Attitude Estimate

The measurement residuals, that is, the difference between the measured quantity and the expected (modeled) quantity, are a good indication of Kalman filter performance. Figures 14 and 15 show a typical 1-h period in the observing mode at L_2 for the DSS and the AST, respectively. Much of the DSS residual is dominated by measurement noise, but all axes show oscillations with both the spin period and the precession period. The AST residuals show the expected measurement noise of a few arc seconds on the $\boldsymbol{x}_B$ and $\boldsymbol{z}_B$ axes and a few tens of arc seconds on the $\boldsymbol{y}_B$ axis, the tracker boresight. The AST $\boldsymbol{x}_B$-axis and $\boldsymbol{y}_B$-axis residuals also exhibit spin-period oscillations with 30-arc-s amplitude, about 90 deg out of phase with each other. In addition, the residuals on the AST $\boldsymbol{x}_B$ axis, which is perpendicular to the AST boresight, have 15-arc-s jumps near each peak. These oscillations and jumps arise from residual sensor misalignments, approximations in propagating the attitude between measurements, and small uncertainties in time-tagging the measurements, which all have a large effect for spinning spacecraft. Based on the definitive ground attitude solution, the WMAP attitude determination accuracy (root sum square of Kalman filter error and systematic error) is 1.1 arc-s (x and z, perpendicular to the AST boresight) and 5.3 arc-s (y, around boresight), all 1σ. Because this easily meets the pointing knowledge requirement of 1.3 arc-min per axis (1σ), no further effort was expended in reducing the measurement residuals.

Drift Bias Estimate

WMAP was launched with vendor-supplied default gyro drift bias values loaded in a flight software table. These default values were used to remove the expected gyro drift bias during IRU sensor data processing. The Kalman filter estimates corrections to these table values, and those corrections, the estimated biases, are removed from the IRU rates as well. After the filter was first enabled and converged the day after launch, the estimated drift rates were added to the default drift rates and loaded into the IRU table onboard. The filter was reset so that it would only have to estimate small corrections to the new table drift rates. The total gyro biases have remained stable since launch, indicating good gyro health. In fact, the current estimates for the total gyro biases (default table values plus current Kalman filter estimate) are $[-10.9, 1.4, 7.3]$ deg/h and are within 0.25 deg/h of the total estimates that were loaded the day after launch. The oscillations seen in the $\boldsymbol{x}_B$-axis and $\boldsymbol{y}_B$-axis Kalman filter estimates and the larger bias seen in the $\boldsymbol{z}_B$-axis estimate (shown in Fig. 16) suggest a small error in the IRU scale factor, rather than an actual variation of the sensor data.

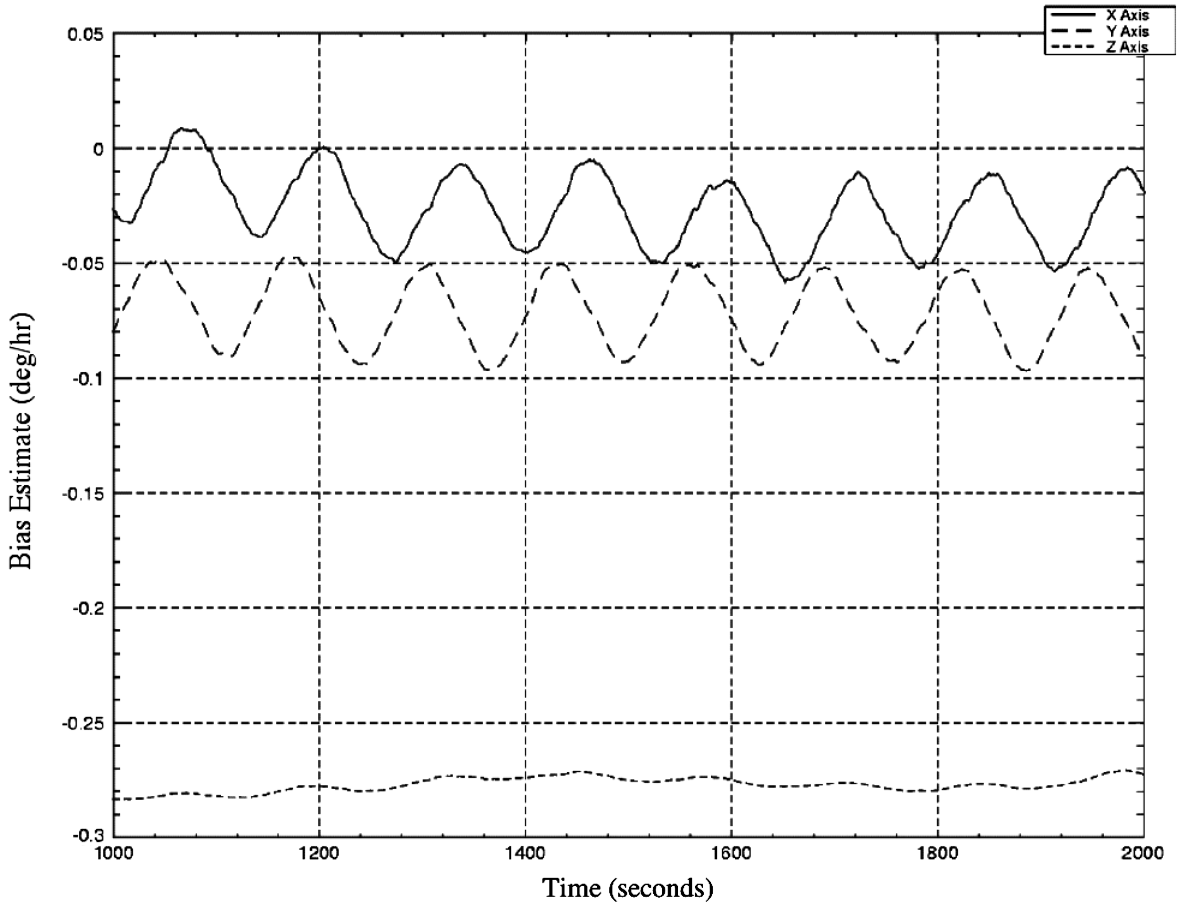

Fig. 16 Kalman filter estimates of gyro bias.

Conclusions

The WMAP spacecraft has to meet stringent attitude control requirements while acquiring the sun, slewing, and performing the compound spin necessary to meet the mission science objectives. The ACS described in this paper has successfully met these demanding requirements far from the Earth, where no magnetic field is useful for sensing or actuation, and with infrequent telemetry passes. Processor upsets in 2001 and 2003 illustrated the importance of having a safemode control capability that is independent of the primary control hardware and software. The flight results show that the WMAP ACS meets or exceeds every requirement.

References

[1]Boggess, N. W., Mather, J. C., Weiss, R., Bennett, C. L., Cheng, E. S., Dwek, E., Gulkis, S., Hauser, M. G., Janssen, M. A., Kelsall, T., Meyer, S. S., Moseley, S. H., Murdock, T. L., Shafer, R. A., Silverberg, R. F., Smoot, G. F., Wilkinson, D. T., and Wright, E. L., "The *COBE* Mission: Its Design and Performance Two Years After Launch," *Astrophysical Journal*, Vol. 397, No. 2, 1992, pp. 420–429.

[2]Gulkis, S., Lubin, P. M., Meyer, S. S., and Silverberg, R. F., "The Cosmic Background Explorer," *Scientific American*, Vol. 262, No. 1, 1990, pp. 132–139.

[3]Smoot, G. F., Bennett, C. L., Kogut, A., Wright, E. L., Aymon, J., Boggess, N. W., Cheng, E. S., De Amici, G., Gulkis, S., Hauser, M. G., Hinshaw, G., Jackson, P. D., Janssen, M., Kaita, E., Kelsall, T., Keegstra, P., Lineweaver, C., Loewenstein, K., Lubin, P., Mather, J., Meyer, S. S., Moseley, S. H., Murdock, T., Rokke, L., Silverberg, R. F., Tenorio, L., Weiss, R., and Wilkinson, D. T., "Structure in the *COBE* Differential Microwave Radiometer First-Year Maps," *Astrophysical Journal Letters*, Vol. 396, Sept. 1992, pp. L1–L5.

[4]Bennett, C. L., Banday, A. J., Gorski, K. M., Hinshaw, G., Jackson, P., Keegstra, P., Kogut, A., Smoot, G. F., Wilkinson, D. T., and Wright, E. L., "Four-Year *COBE* DMR Cosmic Microwave Background Observations: Maps and Basic Results," *Astrophysical Journal Letters*, Vol. 464, 1996, pp. L1–L4.

[5]Bennett, C. L., Bay, M., Halpern, M., Hinshaw, G., Jackson, C., Jarosik, N., Kogut, A., Limon, M., Meyer, S. S., Page, L., Spergel, D. N., Tucker, G. S., Wilkinson, D. T., Wollack, E., and Wright, E. L., "The Microwave Anisotropy Probe Mission," *Astrophysical Journal*, Vol. 583, Jan. 2003, pp. 1–23.

[6]Bennett, C. L., Halpern, M., Hinshaw, G., Jarosik, N., Kogut, A., Limon, M., Meyer, S. S., Page, L., Spergel, D. N., Tucker, G. S., Wollack, E., Wright, E. L., Barnes, C., Greason, M. R., Hill, R. S., Komatsu, E., Nolta, M. R., Odegard, N., Peiris, H. V., Verde, L., and Weiland, J. L., "First-Year Results from *WMAP*," *Astrophysical Journal Supplement Series*, Vol. 148, Sept. 2003, pp. 1–241.

[7]Richon, K. V., and Mathews, M. W., "An Overview of the Microwave Anisotropy Probe (MAP) Trajectory Design,"*Astrodynamics 1997*, edited by F. R. Hoots, B. Kaufman, P. J. Cefola, and D. B. Spencer, Vol. 97, Advances in the Astronautical Sciences, Univelt, San Diego, CA, 1998, pp. 1979–1998.

[8]Cuevas, O., Kraft-Newman, L., Mesarch, M., and Woodard, M., "An Overview of Trajectory Design Operations for the Microwave Anisotropy Probe Mission," AIAA Paper 2002-4425, 2002.

[9]Mesarch, M., Rohrbaugh, D., and Schiff, C., "Contingency Planning for the Microwave Anisotropy Probe Mission," AIAA Paper 2002-4426, 2002.

[10]Mesarch, M., and Andrews, S., "The Maneuver Planning Process for the Microwave Anisotropy Probe (MAP) Mission," AIAA Paper 2002-4427, 2002.

[11]Edery, A., "Earth Shadows and the SEV Angle of MAP's Lissajous Orbit at L_2," AIAA Paper 2002-4428, 2002.

[12]Rohrbaugh, D., and Schiff, C., "Station-Keeping Approach for the Microwave Anisotropy Probe (MAP)," AIAA Paper 2002-4429, 2002.

[13]Andrews, S. F., Campbell, C. E., Ericsson-Jackson, A. J., Markley, F. L., and O'Donnell, J. R., Jr., "MAP Attitude Control System Design and Analysis," *Flight Mechanics Symposium 1997*, NASA CP-3345, Goddard Space Flight Center, Greenbelt, MD, 1997, pp. 445–456.

[14]Ericsson-Jackson, A. J., Andrews, S. F., O'Donnell, J. R., Jr., and Markley, F. L., "MAP Stability, Design and Analysis," *Spaceflight Dynamics 1998*, edited by T. H. Stengle, Vol. 100, Advances in the Astronautical Sciences, Univelt, San Diego, CA, 1998, pp. 955–969.

[15]Markley, F. L., Andrews, S. F., O'Donnell, J. R., Jr., and Ward, D. K. "The Microwave Anisotropy Probe (MAP) Mission," AIAA Paper 2002-4578, 2002.

[16]Ward, D. K., Davis, G. T., and O'Donnell, J. R., Jr., "The Microwave Anisotropy Probe Guidance, Navigation, and Control Hardware Suite," AIAA Paper 2002-4579, 2002.

[17]Andrews, S. F., and O'Donnell, J. R., Jr., "MAP Attitude Control System Design and Flight Performance," AIAA Paper 2002-4580, 2002.

[18]VanBezooijen, R. W. H., Anderson, K. A., and Ward, D. K., "Performance of the AST-201 Star Tracker for the Microwave Anisotropy Probe," AIAA Paper 2002-4582, 2002.

[19]O'Donnell, J. R., Jr., Davis, G. T., and Ward, D. K., "Restoring Redundancy to the Wilkinson Microwave Anisotropy Probe Propulsion System," *Journal of Spacecraft and Rockets*, Vol. 42, No. 2, 2005, pp. 336–344.

[20]Starin, S., and O'Donnell, J. R., Jr., "Development of a Two-Wheel Contingency Mode for the MAP Spacecraft," AIAA Paper 2002-4584, 2002.

[21]Wertz, J. R. (ed.), *Spacecraft Attitude Determination and Control*, D. Reidel, Dordrecht, The Netherlands, 1978, Chaps. 12, 16, and 17, Appendices D and E.

[22]Shuster, M. D., "A Survey of Attitude Representations," *Journal of the Astronautical Sciences*, Vol. 41, No. 4, 1993, pp. 439–517.

[23]Lefferts, E. J., Markley, F. L., and Shuster, M. D., "Kalman Filtering for Spacecraft Attitude Estimation," *Journal of Guidance, Control, and Dynamics*, Vol. 5, No. 5, 1982, pp. 417–429.

[24]Murrell, J. W., "Precision Attitude Determination for Multimission Spacecraft," *1978 AIAA Guidance and Control Conference*, AIAA, New York, 1978, pp. 70–87.

[25]Bauer, F. H., Femiano M. D., and Mosier, G. E., "Attitude Control System Conceptual Design for the X-ray Timing Explorer," AIAA Paper 92-4334, 1992.

[26]Mortensen, R. E. "A Globally Stable Linear Attitude Regulator," *International Journal of Control*, Vol. 8. No. 3, 1968, p. 297.

[27]Wie, B., and Barba, P. M., "Quaternion Feedback for Spacecraft Large Angle Maneuvers," *Journal of Guidance, Control, and Dynamics*, Vol. 8, No. 3, 1985, pp. 360–365.

[28]Psiaki, M., "Estimation of a Spacecraft's Attitude Dynamics Parameters Using Flight Data," *Journal of Guidance, Control, and Dynamics* (to be published); also *Flight Mechanics Symposium 2003*, NASA CP-2003-212246, Goddard Space Flight Center, Greenbelt, MD, 2003.

[29]Starin, S., O'Donnell, J. R., Jr., Ward, D. K., Wollack, E. J., Bay, P. M., and Fink, D. R., "Anomalous Force on the Wilkinson Microwave Anisotropy Probe," *Journal of Spacecraft and Rockets*, Vol. 41, No. 6, 2004, pp. 1056–1062.